Journal of Engineering and Technological Sciences

Research Paper

Design and Characterization of Ultrasonic Langevin Transducer 20 kHz Using a Stepped Horn Front-Mass

Aisyah Nurul Khairiyah[1], Gandi Sugandi[2] & Deddy Kurniadi[3]

[1]Instrumentation and Control Master Program, Faculty of Industrial Technology, Institut Teknologi Bandung, Jalan Ganesa No.10 Bandung 40132, Indonesia
[2]Research Center for Electronics – National Research and Innovation Agency (BRIN), KST Samaun Samadikun, Jalan Sangkuriang, Bandung 40135, Indonesia
[3]Instrumentation and Control Research Group, Faculty of Industrial Technology, Institut Teknologi Bandung, Jalan Ganesa No.10 Bandung 40132, Indonesia

Corresponding author: nurul415@gmail.com

Abstract

Ultrasonication is a method that is widely used in various fields. One of its applications is to accelerate the process of homogenization, emulsification, and extraction. In the ultrasonicator system, the transducer is an extremely important device. The resonant frequency, longitudinal vibration amplitude, and electromechanical coupling are the targets in designing an ultrasonic transducer. In this investigation, the main contribution was the development of a simple and effective method for mechanically tuning the resonant frequency of the transducer by adding mass to the front end of the mass or stepped horn. This study also aimed to obtain optimal results by examining the effects of geometric dimensions, bolt prestress, stress distribution, resonant frequency, amplitude, and electrical impedance. The ultrasonic transducer model was designed with a resonant frequency of 20 kHz and simulated using the finite element analysis. The steps involved included calculating the dimensions and geometric structure of the transducer, modeling using the finite-element method, and experimental validation. The simulation results and measurements showed that the series resonant frequency, electrical impedance, and effective electromechanical coupling of the Model-4 transducer 16·13 mm radiator configuration were 20.15 kHz, 100 Ω, and 0.2229 from the simulation results, and 20.17 kHz, 24.91 Ω, and 0.2033 from the measurement results. A percentage difference, or relative error, of 0.1% was obtained between the simulation and the experimental results for this Model-4 with bolt prestressing at 15 kN.

Keywords: *bolt-clamped Langevin transducer; effective electromechanical coupling coefficient; finite element analysis; resonance characteristics; ultrasonication.*

Introduction

Ultrasonic or sonication systems are widely applied in the medical field (dental ultrasonic scalers – Engelke and Oehme [1] and Li *et al*. [2]); industry (welding, cutting, machining – Milewski et al. [3]); and accelerating chemical processes (homogenization, emulsification, extraction, dispersion, and particle reduction – Batista [4]). The sonication system consists of an electrical signal generator, an ultrasonic transducer, and a horn or sonotrode, directly contacting the sample to be processed. The bolt clamped Langevin transducer (BCLT) is an ultrasonic transducer that can convert electrical wave energy into mechanical waves or vice versa. The resulting mechanical wave vibrations are generally in the form of longitudinal waves. The longitudinal wave vibrations generated by the BCLT transducer are usually designed at frequencies above 20 kHz (ultrasonic waves). The structural arrangement of this transducer consists of two or more piezoelectric ceramics as the active elements clamped by two metal blocks, namely the front and back mass, electrodes, and bolts. The four main components are assembled and the bolts are tightened in such a way that all the parts that make up the transducer are firmly bonded together without leaving gaps between the component surfaces.

The resonant frequency, electrical impedance, longitudinal vibration amplitude, and electromechanical coupling are the main characteristics of the BCLT that need to be considered in the transducer design process. Parameters

ISSN: 2337-5779
J. Eng. Technol. Sci. Vol. 55, No. 3, 2023, 357-372
DOI: 10.5614/j.eng.technol.sci.2023.55.4.1

that significantly affect the ultrasonic transducer's performance are material selection, geometric structure, and bolt prestressing, as well as the mechanical resistance of the ultrasonic transducer. Bolt prestress affects the resonant frequency, electrical impedance, and vibration amplitude, as well as the effective electromechanical coupling of the transducer.

Several studies have reported this, such as Kim and Lee [5,6], Fu *et al*. [7], and Arnold and Martins [8], which state that bolt prestressing in the transducer assembly causes the resonance frequency position to change and shift up as the applied prestress increases. Meanwhile, DeAngelis et al. [9] states that prestressing bolts not only changes the transducer characteristics but can also be used to optimize transducer performance.

In addition to pre-tensioning bolts, the geometric structure of the transducer can also affect the performance of the transducer. This has been reported by Abdullah *et al*. [10], Baraya and Hossam [11], and Haili *et al*. [12], who concluded that every geometric shape that makes up the transducer is able to shift the location of the transducer resonant frequency. A dimensional or structural element that is usually adjusted when designing a transducer is the front mass. A stepped horn shape can be used to amplify the amplitude of the vibration at the end of the front mass.

Based on the results of previous investigations, we aimed to obtain a comprehensive methodology in designing a complex Langevin transducer. Several parameters, i.e., bolt prestress, geometric structure, clearly affect the main performance of the transducer, which includes the resonant frequency and the vibration amplitude. Increasing the magnitude of the transducer vibration amplitude is generally done by reducing the front-mass diameter to a stepped horn shape, however, this can increase the resonant frequency. Therefore, the main contribution of this work was the development of a simple and effective method for mechanically tuning the resonant frequency of the transducer by adding mass to the front end of the mass or stepped horn. The methodology used in the investigation included simulations using finite element analysis (FEA) and validation by experimental measurements. Several of the main criteria to be achieved in this study were the accuracy of the resonance frequency, the electromechanical coupling coefficient, and the vibration amplitude. In the geometric dimension design of the transducer, the length of each section was calculated according to the half-wavelength device method. In contrast, the size of the piezoelectric active element material was fixed. From the results of the calculation of these dimensions, simulations were carried out using commercial software based on finite element analysis and Comsol-Multiphysics version 5.6.

In addition, the effects of changes in the diameter of the stepped horn and the bias were also simulated and analyzed for their effects on changes in the resonant frequency and the magnitude of the transducer vibration amplitude by considering the stress distribution that occurs in the transducer, especially in ring-shaped piezoelectric ceramics. The magnitude of the stress distribution on the piezoelectric ring is also a major concern, in order to obtain a safe and efficient transducer performance. After getting optimal results from the simulation results, the next step was transducer fabrication for experimentation and validation of the results. In the experimental stage, the characteristics of the transducer were measured, including the resonant frequency and electrical impedance to variations in the application of prestressing to the bolts.

Materials and Methods

Transducer Structure and Materials

The general geometric structure of an ultrasonic transducer is shown in Figure 1. The design in Figure 1(a) shows the geometric structure of an ultrasonic transducer with a constant diameter for the back and front masses. Meanwhile, Figure 1(b) shows a transducer geometry structure with different diameter. The diameter difference between the back and front mass block was designed to obtain a gain in vibration amplitude at the front end of the front mass block. Figure 1(b) shows the transducer model that was tested and verified experimentally in this study.

DOI: 10.5614/j.eng.technol.sci.2023.55.4.1

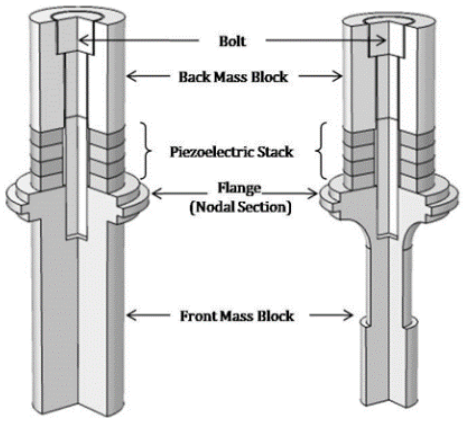

Figure 1 Geometry of a symmetric ultrasonic transducer with (a) constant diameter and (b) a step-horn type structure.

In the design of a transducer, material selection is the first aspect that must be done. In addition, the mechanical properties of the material must also be considered. The material mechanical properties can affect the ultrasonic transducer performance. Studies by DeAngelis *et al.* [9], Baraya and Hossam [11], Qiao and Wang [13], DeAngelis *et al*. [14], and Pérez-Sánchez *et al.* [15] state that the best materials are stainless steel (AISI 4340 and SS-304), piezoelectric PZT-4, and aluminum (Al 7075-T6) and bolt (SS-304 Steel alloy DIN912 class 12.9).

Transducer Geometry Calculation

The total length of the transducer can be calculated according to the wavelength of the longitudinal wave velocity of sound in each of the materials used to construct the transducer. The desired resonance working frequency of the transducer can be used to determine the wavelength, where the wavelength is equal to the speed of sound in the material divided by the desired resonance frequency.

To measure the lengths of the components, the proposed model for the transducer structure is shown in Figure 2. It is widely applied by positioning the piezoelectric ceramic stack away from the nodal location to ensure that the resulting displacement is not affected by the nodal location. This action is taken to improve the performance of the piezoelectric stack. Each quarter wavelength can be calculated individually using Eqs. (1) and (2). Eq. (1) is used to calculate the quarter wavelength on the left and Eq. (2) for the right of the nodal location (Xu and Huanhuan [16]).

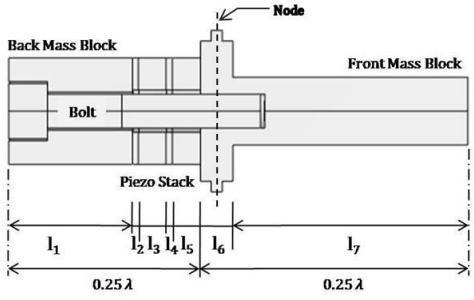

Figure 2 Division of the ultrasonic transducer area to be calculated.

$$\frac{Z_1}{Z_3}\tan k_1 l_1 \tan k_3 l_3 + \frac{Z_1}{Z_5}\tan k_5 l_5 \tan k_1 l_1 + \frac{Z_3}{Z_5}\tan k_3 l_3 \tan k_5 l_5 = 1 \quad (1)$$

$$\frac{Z_7}{Z_6}\tan k_6 l_6 \tan k_7 l_7 = 1 \quad (2)$$

Meanwhile, the value of the acoustic impedance of each material denoted by Z_1 to Z_7 can be calculated using Eq. (3).

$$Z = \rho C A \quad (3)$$

ρ, C and A are the mass density, speed of sound, and surface area of the structure and material used in the transducer, and k is the wave number equal to the angular frequency ω divided by the sound speed C in the material $k = 2\pi f/C$ or $k = 2\pi/\lambda, \lambda\lambda$ is the wavelength.

Prestressing the bolt on a Langevin transducer is an important step to ensure secure operation of the piezoelectric element when compression stress is applied during assembly. The objective of prestressing is to achieve maximum power and an effective contact area between the transducer elements, while preventing displacement during operation. Proper prestress control is crucial for the lifespan, maximum operation power, and efficiency of the ultrasonic transducer and converter. Excessive prestress can alter the properties of the piezoelectric material and may lead to crushing. On the other hand, insufficient prestress can allow lateral displacement of the piezo-ceramic rings, especially at high power level, which can result in crack, electric arcs, or short circuits.

The optimal prestress value depends on factor such as the compression strength of the piezoelectric material and the static pressure distribution on the piezoelectric ceramic rings. Typically, the static pressure is highest near the inner edge, close to the bolt, and decreases symmetrically in a circular pattern toward the outer edge of the piezo-ceramic rings.

For the specific piezoelectric material PZT-4, the recommended optimum prestress value falls within a range of 20 to 40 MPa (Abdullah *et al* [10] and Baraya and Hossam [11]). Thus, the bolt load can be calculated so that the tensile load on the bolt equals the compressive load on the stack. Under static conditions, the tensile force on the bolt is equal to the compression force on the piezoelectric ceramic, as expressed in Eq. (4):

$$\frac{T_{ob}}{T_{oc}} = \frac{A_c}{A_b} \tag{4}$$

T_{ob} and T_{oc} are the axial stresses in the bolt and the piezoelectric ceramic, respectively. Meanwhile, A_b and A_c are in the cross-sectional area of the piezoelectric ceramic bolt and ring, respectively.

The front and back block as well as the bolt of the Langevin vibrator are all made of ideal linear elastic materials. The bolt and back mass are made of stainless steel, and the front mass is made of aluminum alloy. The piezoelectric ceramics are made of four piezoelectric ceramic rings polarizing along the z direction. The polarization directions of any two adjacent ceramic rings are opposite. The parameters of the materials are as shown in Table 1.

Table 1 Piezoelectric ceramics (PZT-4), 7075-T6 aluminum, and 304 stainless steel [6,10,17].

Material	Properties		
	Piezoelectric constant matrix (C·m^{-2})	**Elasticity matrix (10^{10}×N·m^{-2})**	**Dielectric constant (F.m^{-1})**
Piezoelectric, PZT-4	$\begin{bmatrix} 15.1 & 0 & 0 \\ -5.2 & 0 & 0 \\ -5.2 & 0 & 0 \\ 0 & 12.7 & 0 \\ 0 & 0 & 0 \\ 0 & 0 & 12.7 \end{bmatrix}$	$\begin{bmatrix} 13.9 & 7.78 & 7.43 & 0 & 0 & 0 \\ 7.78 & 13.9 & 7.43 & 0 & 0 & 0 \\ 7.43 & 7.43 & 11.5 & 0 & 0 & 0 \\ 0 & 0 & 0 & 3.06 & 0 & 0 \\ 0 & 0 & 0 & 0 & 2.56 & 0 \\ 0 & 0 & 0 & 0 & 0 & 2.56 \end{bmatrix}$	$\begin{bmatrix} 762.5 & 0 & 0 \\ 0 & 762.5 & 0 \\ 0 & 0 & 663.2 \end{bmatrix}$

	Properties			
	Density (kg.m^{-3})	Young's modulus (GPa)	Poisson's ratio	Sound velocity (m/s)
Aluminum (7075-T651)	7500	78	0.3	3203
Back-mass 304 stainless steel	71.1	0.33	2810	6210
Front-mass and bolt	205	0.28	7886	5720

To evaluate the energy conversion rate from the electrical source to the mechanical vibration, the effective coupling coefficients k_{eff} of the transducer are calculated from FEA models and experiments based on [6]:

DOI: 10.5614/j.eng.technol.sci.2023.55.4.1

$$k_{eff} = \sqrt{1 - \frac{f_r^2}{f_a^2}} \quad (5)$$

where f_r is the resonant frequency and f_a is the anti-resonant frequency. For comparison of the results between the FEA models and the experiments, the fractional relative error (%) was determined by Eq. (6):

$$\varepsilon(\%) = \left|1 - \frac{f_{r\_FEA}}{f_{r\_exp}}\right| x100 \quad (6)$$

where f_{r_FEA} and f_{r_exp} are the resonant frequency results from the simulation and the experiment, respectively.

Finite Element Modeling

The next step in the transducer design process was to simulate the transducer design using the commercial FEA software COMSOL-Multiphysics version 5.6. In the modeling process, this software provides several alternatives in a simulation, such as modeling in 3-dimensional and 2-dimensional axis symmetry. A 3-dimensional (3D) model simulation uses a lot of computer memory and a relatively long time to analyze. This is due to the rather large number of mesh elements. Meanwhile, for the simulation of a 2-dimensional (2D) axis symmetrical model, besides being efficient in computer memory, the time used is relatively less. This is due to the relatively small mesh formation. In general, simulations using finite element analysis are divided into two processing stages, namely the pre-processing and the post-processing stage, either for 3D or 2D-axisymmetric models, as shown in Figure 3. In this work, the simulation used a 2D-axisymmetric model to obtain fast results and relatively low memory usage. In this bolt-clamped Langevin transducer simulation, the appropriate modules used included solid mechanics and electrostatic modules.

During the pre-processing stage, the geometry of the transducer was defined using CAD software or FEA modeling tools. The dimensions and shape of the transducer, including piezoelectric ceramic rings, back-mass and front-mass or step-horn elements, and the bolt clamping mechanism, were carefully specified (Figure 3(a)(1)). The 2D-axisymmetric model simplifies the geometry by considering only a single cross-sectional slice and assuming rotational symmetric around the central axis.

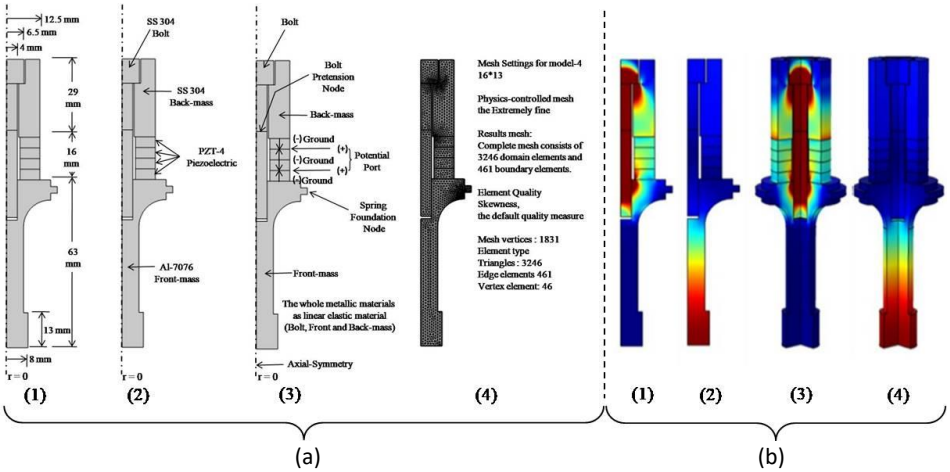

Figure 3 Stages of the piezoelectric ultrasonic transducer simulation process using the finite element method (a) pre-processing and (b) post-processing or optimization with visualization in 2D or 3D.

Following geometry creation, the materials properties were assigned to the transducers components. This involves specifying the properties of the piezoelectric material, including piezoelectric coefficients, elastic constant, and dielectric properties. The material properties of the back and front mass (stainless steel SS304 and aluminum Al-7075-T6) involve Young's modulus, density, poison ratio, and sound velocity. The metallic materials, which provide structural support, and the bolt (stainless steel) used for clamping were also assigned respective material properties, as shown in Figure 3(a)(2).

Boundary conditions and excitations were defined to replicate the real operating conditions of the transducer. Spring-foundation supports and clamping conditions for the bolts were specified, mimicking the physical setup. The appropriate excitation, such as electrical voltage and ground node, was applied to the piezoelectric elements to simulate their response and generate the desired output (Figure 3(a)(3)). The input voltage given to the piezoelectric ceramic was 1 V_{rms} with a frequency sweep in the range of 18 kHz to 23 kHz, with a step of 10 Hz.
A mesh was generated for the 2D-axisymmetric model. The mesh accurately represented the transducer geometry, ensuring that critical features and phenomena were captured. It is essential to determine an appropriate mesh density, especially in areas of interest such as the piezoelectric elements and clamping region, to accurately model the stress distribution and vibrations. The mesh setting for the Model-4 transducer was 'physics-controlled mesh with extremely fine element quality skewness as the default quality measure. The complete mesh consisted of 3,246 domain elements and 461 boundary elements, for example, the meshing result of Model-4 16*13 (Figure 3(a)(4)). After running the simulation, the post-processing stage was conducted to determine the transducer performance, including stationary simulations to find the solution to linear and nonlinear in static or steady-state problem. This step was done to determine the prestress distribution of all materials, especially the piezoelectric materials. The next stage was a study of the condition in the frequency domain. This stage was carried out to determine the effect of prestressing on changes in resonance frequency, the impedance response to frequency, and the electromechanical coupling factor.

The simulation results provide insight into the transducer behavior and characteristics. Stress distribution analysis enables the evaluation of the structural integrity of the transducer by identifying regions of high stress concentration (Figure 3(b)(1) and 3(b)(3) for 2D-axisymmetric and 3D rotational results respectively). The displacement field analysis helps to understand the transducer vibrational behavior and identify its mode shapes and resonance frequencies (Figure 3(b)(2) and 3(b)(4) respectively for 2D-axisymmetric and 3D rotational results). The electric potential distribution analysis allows the assessment of the transducer's electrical response, impedance characteristics, and frequency response.

Simulation and Analysis

In the simulation, four models of simulated geometric structures were used. These were created to see their effect on the performance of the transducer. The observed effects were the distribution of prestress, resonance frequency, and impedance response. The models were made as shown in Figure 4 below. Model-1 in Figure 4(a) is a transducer with a structure that has a constant diameter. Model-2 in Figure 4(b) is a transducer with front-mass and back-mass geometric designs with different diameters. Model-2 is often called a transducer with a step-horn structure. Model-3 in Figure 4(c) is a transducer with the same geometric structure as Model-2 but with an additional radius in the transition area of the front mass horn. Model-4 is the same as Model-3 with a radiator structure added at the front-mass end, as shown in Figure 4(d). Model-4 has an additional radiator structure at the end of the horn with the same diameter but a different height; this structure adds some mass to the front end of the transducer.

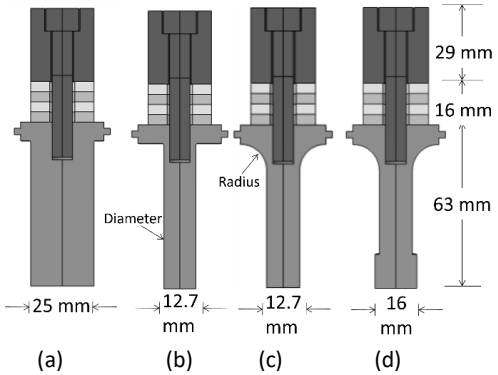

Figure 4 The studied transducer models with different geometric structures: (a) constant diameter transducer, (b) transducer with different front mass diameter geometries, (c) transducer with addition of radius at the front mass transition, and (d) transducer with radiator addition.

DOI: 10.5614/j.eng.technol.sci.2023.55.4.1

The four models with the structures and dimensions shown in Figures 4 (a) to 4(d) were simulated and studied for their effect on the transducers performance. The parameters studied included the geometric structure and the impact of prestressing on transducer performance with variation of the prestress values on the bolts at 10 kN, 15 kN, 20 kN, and 25 kN. The transducer performance included the stress distribution when prestressing the bolt, resonance frequency (eigenfrequency), harmonic frequency, and impedance. In the harmonic frequency and impedance simulation stage, the frequency sweep given to the transducer was in the 18 kHz to 24 kHz range, with steps of 10 Hz. The electric potential given to the piezoelectric electrode was 1 V_{rms}.

Simulation and Analysis Model-1

The results of the ultrasonic transducer simulation for Model-1 at the beginning of this study are shown in Figure 1. The size of the ultrasonic transducer used was based on the results of calculations with Eqs. (1) and (2). Referring to the recommendation that a safe pressure for piezoelectric ceramics is between 20 MPa and 40 MPa, the simulation results show that the tension forces on the bolts were in the range of 10 kN and 15 kN, as shown in Figure 5(a) and Figure 5(b). The stress obtained was above 10 MPa to 40 MPa. Based on Eq. (4) for a bolt diameter of 8 mm and a piezoelectric ring with an outer diameter of 25 mm and an inner diameter 10 mm, for bolt pretension at 15 kN, a tension stress in the piezoelectric ceramics of 36 MPa was obtained. Meanwhile, for prestress at 20 kN and a stress distribution of 25 kN, especially at the location of the piezoelectric ceramics, the stress obtained was above 40 MPa to 100 MPa. This condition would damage the transducer when dynamically run.

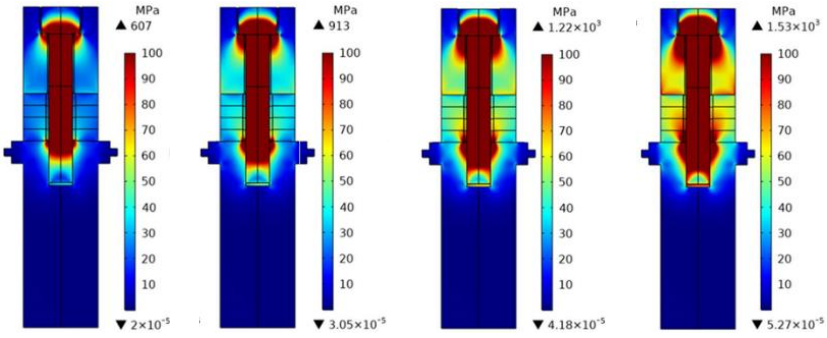

(a) 10 kN (b) 15 kN (c) 20 kN (d) 25 kN

Figure 5 Simulation results of stress distribution on the Model-1 ultrasonic transducer with various bolt prestress values.

Figure 6 shows the impedance response curve to changes in frequency, Figure 6(a) and the magnitude of the vibration amplitude Figure 6(b) on the transducer with various bolt prestress values, ranging from 10 kN, 15 kN, 20 kN, to 25 kN. The difference in prestressing of the bolt produces changes in the resonance frequency, impedance, and vibration amplitude at the end of the horn.

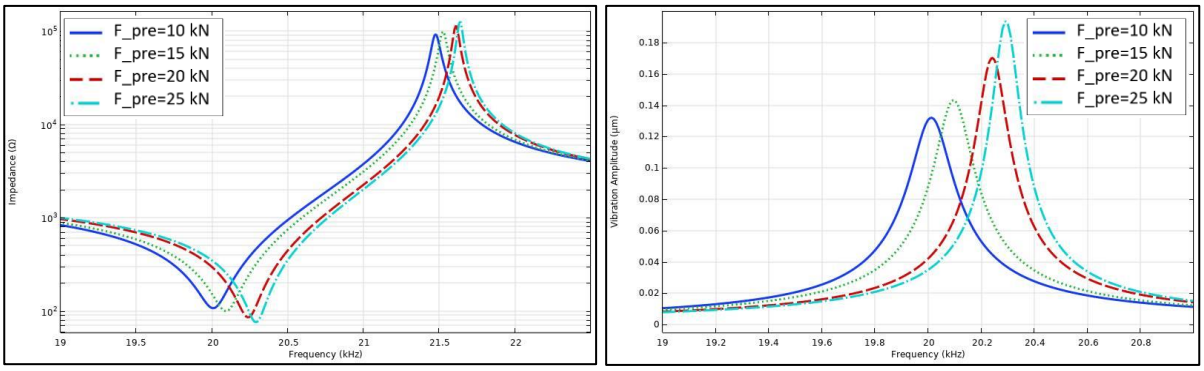

(a) (b)

Figure 6 Graph of the simulation: (a) results of frequency response to impedance and (b) vibration amplitude on transducer Model-1 for different prestress forces of 10 kN (blue solid line), 15 kN (green dotted line), 20 kN (red dashed line), and 25 kN (cyan dashdot line).

As a result of applying pressure to the bolt, there was a shift in the value of its resonance and antiresonance frequencies, as well as changes in the impedance and vibration amplitude values. As the prestress increased, the resonance frequency and vibration amplitude increased as well. At the same time, the value of the impedance at the resonance frequency decreased and vice versa. At the antiresonance frequency, the impedance increased. The importance of these changes is shown in detail in Table 2.

Table 2 Value of the resonance frequency and impedance and amplitude of the vibration of Model-1.

Prestress force (kN)	f_r (kHz)	Z_r (Ω)	f_a (kHz)	Z_a (kΩ)	Eigen-frequency (kHz)	Amplitude at f_r /1V_{rms} (μm)	Electro-mechanical coupling factor, k_{eff}.
10	19.95	107.1	21.45	93.332	19.947	0.130	0.3674
15	20.04	99.79	21.5	99.424	20.033	0.142	0.3622
20	20.19	85.52	21.59	115	20.182	0.168	0.3542
25	20.24	75.69	21.62	127	20.235	0.192	0.3515

*Resonance frequency (f_r), antiresonance (f_a), Impedance in f_r (Z_r), Impedance in f_a (Z_a).

Simulation and Analysis of Model-2

The subsequent investigation was to study the diameter changes of the stepped horn front mass with diameters varying from 19 mm, 16 mm to 12.7 mm. The goal to be achieved with this front configuration is to increase or amplify the vibration amplitude at the end of the horn. The results of the transducer simulation with a prestress of 15 kN showed that the stress distribution in Model-2 was starting to show changes in stress at the location of the connection between the large and small diameter stepped front mass horn. When the diameter of the horn was smaller, it resulted in more significant stress at the junction, which would cause damage to this part. The stress distribution with a prestress of 15 kN is shown in Figure 7.

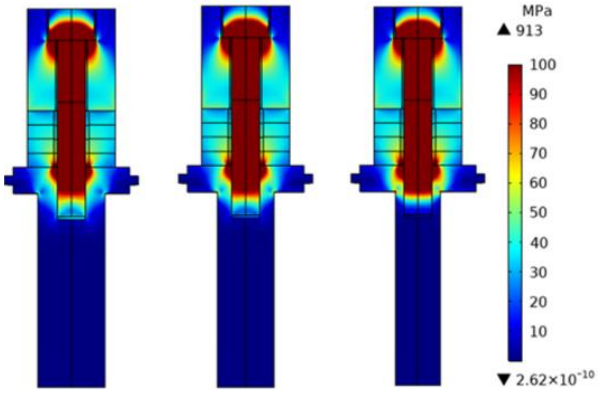

(a) 19 mm (b) 16 mm (c) 12.7 mm

Figure 7 Simulation results of the stress distribution of the transducer with variations in the diameter of the horn at a bolt prestress value of 15 kN.

Meanwhile, there was a change in the resonance frequency. The smaller the horn diameter, the more the resonance and impedance shifted upward. The changes that occurred in the antiresonance frequency and its impedance shift decreased, as shown in Figure 8(a), and the magnitude of the vibration amplitude Figure 8(b) on the transducer with a bolt prestress value of 15 kN. Because the distance between the resonance and antiresonance frequencies was getting smaller, the electromechanical coupling of the transducer decreased, but the amplitude of the resulting vibration increased. The values of the resonance and antiresonance frequencies, impedance, eigenfrequency, vibration amplitude, and electromechanical coupling factor are shown in Table 3.

DOI: 10.5614/j.eng.technol.sci.2023.55.4.1

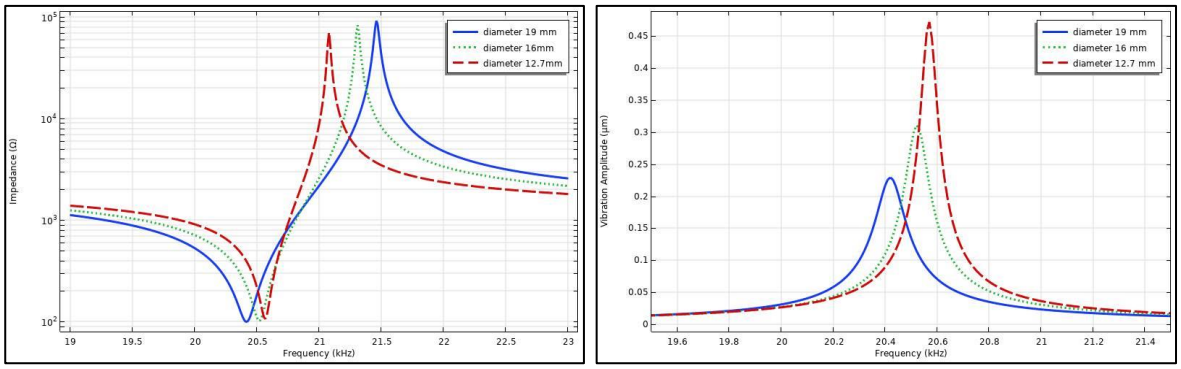

(a) (b)

Figure 8 Graph of simulation results of: (a) frequency response to electrical impedance and (b) vibration amplitude on the Model-2 transducer with diameters of 19 mm (blue solid line), 16 mm (green dotted line), and 12.7 mm (red dash line) on a 15 kN prestressed bolt.

Table 3 Value of the resonance frequency and impedance and amplitude of the vibration of Model-2 at 15 kN prestress.

Diameter stepped-horn (mm)	f_r (kHz)	Z_r (Ω)	f_a (kHz)	Z_a (kΩ)	Eigen-frequency (kHz)	Amplitude at f_r /1Vrms (μm)	Electro-mechanical coupling factor, k_{eff}.
19	20.42	99.31	21.46	91.64	20.416	0.229	0.3075
16	20.52	101.40	21.31	82.74	20.519	0.310	0.2698
12.7	20.57	106.69	21.11	78.22	20.565	0.472	0.2186

Simulation and Analysis of Model-3

Based on the results shown in Section 3.2, in the stepped shape in the front-mass junction, there was a significant distribution of stress that could damage the intersection. Therefore, to reduce the stress on the stepped hub, it is necessary to increase the radius of the fillet junction. Figure 9 shows the simulation results of the stress distribution at the step-junction section where stress reduction occurred. The fillet radii starting from 5 mm, 7.5 mm, and 10 mm indicated that the larger the radius, the less fillet stress occurred.

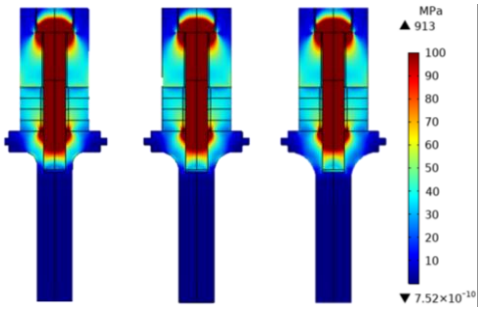

(a) (b) (c)

Figure 9 Simulation results of the stress distribution of the Model-3 transducer with a fillet radius of (a) 5 mm, (b) 7.5 mm, and (c) 10 mm on a bolt prestressed at 15 kN.

Figure 10(a) shows the impedance and resonance response curves and the magnitude of the vibration amplitude (Figure 10(b)) on the transducer with various bolt prestress values 15 kN due to the influence of these fillet-radius parameters. It turned out that this fillet radius had a massive impact on the resulting resonance frequency. From the simulation results, the resonance frequency shifted to above 20 kHz, which was the target, namely 21.16 kHz, 21.62 kHz, and 22.15 kHz for an increase in radius of 5 mm, 7.5 mm, and 10 mm, respectively, with decreasing impedance.

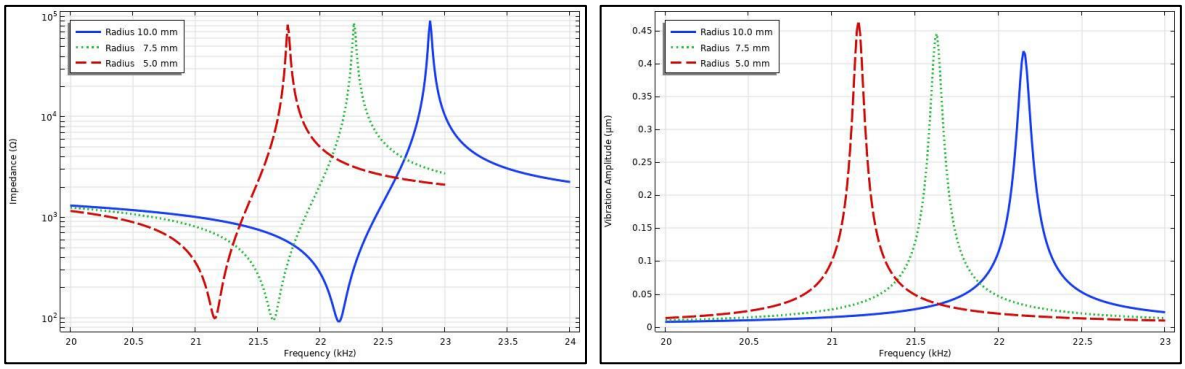

(a) (b)

Figure 10 Simulation results of the Model-3 transducer (a) electrical impedance and (b) vibration amplitude with a 10-mm (solid blue line), 7.5-mm (dotted green line), and 5-mm (red dash line) fillet radius on a 15 kN prestressed bolt.

Likewise, the antiresonance frequency changed to 21.74 kHz, 22.27 kHz, and 22.88 kHz, and the impedance also increased. Table 4 shows the values of the resonance and antiresonance frequencies and their impedances. Meanwhile, the electromechanical coupling factor increased with the fillet radius at the junction, and the vibration amplitude decreased.

Table 4 Values of resonance frequency and impedance and amplitude of Model-3 vibration at 15 kN bolt prestress.

Radius-Fillet (mm)	f_r (kHz)	Z_r (Ω	f_a (kHz)	Z_a (kΩ)	Eigen-frequency (kHz)	Amplitude at f_r /1Vrms (μm)	Electro-mechanical Coupling factor, k_{eff}.
5	21.16	104.410	21.74	79.506	21.157	0.465	0.2294
7.5	21.62	94.498	22.27	85.252	21.625	0.439	0.2398
10	22.15	90.630	22.88	89.580	22.150	0.418	0.2506

Simulation and Analysis of Model-4

Finally, the effect of adding a radiator at the end of the stepped horn front mass on the performance of a transducer designed to produce a resonance frequency of 20 kHz was investigated. Model-4 was divided into three additional geometric structures with radiators measuring in diameter and height 16·23 mm, 16·16 mm, and 16·13 mm. The addition of this radiator was located at the front-mass end. Figure 11 shows the stress distribution results where there was no significant change anymore and the results were the same as those obtained for Model-3.

However, the resonance frequency seemed to change and shift back to a value of around 20 kHz. Figure 12(a) shows the three frequency impedance curves and the magnitude of the vibration amplitude (Figure 12(b)) on the transducer with bolt prestress at 15 kN for the fourth model. Here, we can see the resonance of the addition of radiators for 16·23 mm, 16·16 mm, and 16·13 mm, respectively, to 19.41 kHz, 19.85 kHz, and 20.15 kHz with relative impedance. A decrease in value was observed at 100 Ω for 15 kN prestress. Likewise, the antiresonance frequencies were 19.89 kHz, 20.35 kHz, and 20.67 kHz, with increasing relative impedances of 89.32 kΩ, 97.47 kΩ, and 98.01 kΩ, respectively, under the same prestress conditions. Meanwhile, the electromechanical coupling factor increased with the fillet radius at the junction, and the vibration amplitude relative increased. Detailed results of these are shown in Table 5.

DOI: 10.5614/j.eng.technol.sci.2023.55.4.1

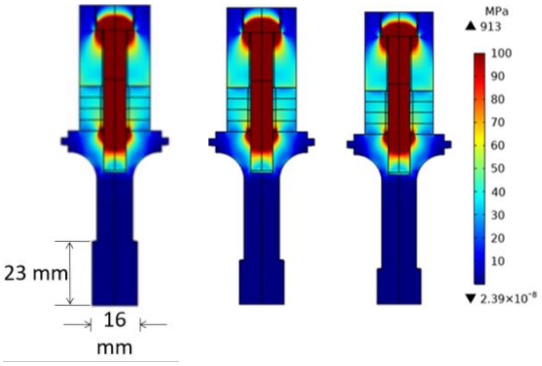

(a) (b) (c)

Figure 11 Simulation results of the stress distribution of the Model-4 transducer with radiator sizes (a) 16·23 mm, (b) 16·16 mm, and (c) 16·13 mm on a 15 kN prestressed bolt.

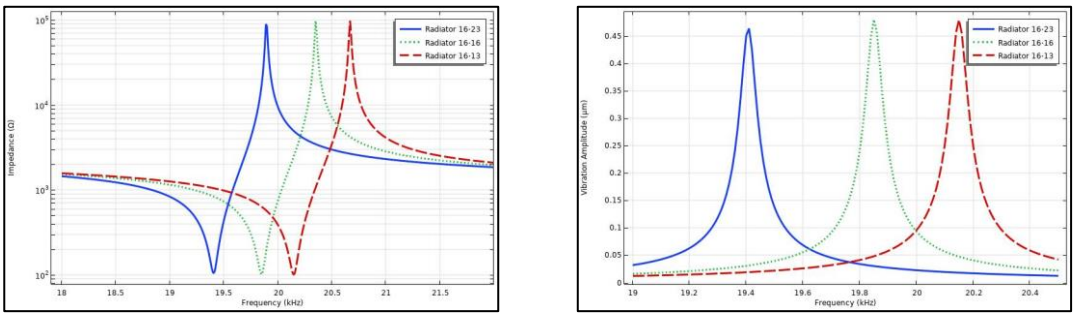

(a) (b)

Figure 12 Simulation results of the Model-4 transducer (a) electrical impedance and (b) vibration amplitude with 16·23 mm (blue-solid), 16·16 mm (green dotted line), and 16·13 mm (red dash line) radiators for a 15 kN prestressed bolt.

Table 5 Value of the resonance frequency and impedance and amplitude of the Model-4 vibration at 15 kN.

Radiator (mm)	f_r (kHz)	Z_r (Ω)	f_a (kHz)	Z_a (kΩ)	Eigen-frequency (kHz)	Amplitude at f_r /1Vrms (μm)	Electro-mechanical coupling factor, k_{eff}.
16·23	19.41	104.97	19.89	89.32	19.408	0.463	0.2184
16·16	19.85	101.44	20.35	97.47	19.849	0.479	0.2203
16·13	20.15	100.10	20.67	98.01	20.148	0.479	0.229

Experiments

According to the simulation results discussed above, the structural geometry of ultrasonic transducer Model-4 with configurations 16·23 mm and 16·13 mm was fabricated for validation, as shown in Figure 13. Both models had a different design, especially at the end of the horn, called the radiator, with a diameter of 16·23 mm (Figure 13(a)) and 16·13 mm (Figure 13 (b)). The piezoelectric ceramic material used, PZT-4, is commercially available in the market, with dimensions according to the simulation. The fabrication process of the structure geometry for back mass and front mass using stainless steel and aluminum, respectively, was done using a lathe work machine. Afterward, all components were assembled and tightened using center bolt M8 using a torque moment meter tool. Using Eq. (4), the torque force given to the bolt was 8 Nm, 16 Nm, and 24 Nm, identical to force values of 5 kN, 10 kN, and 15 kN, respectively.

Based on the simulation results, an ultrasonic transducer geometric design was obtained with a diameter of 12.7 mm, a radius of 10 mm and radiators of 16·23 mm and 16·13 mm. This design was chosen because it produces a resonance frequency value of 20.15 kHz. This value is close to the ultrasonic transducer design target for a resonance frequency of 20 kHz. After that, two prototype ultrasonic transducers were fabricated.

(a) (b)

Figure 13 Fabricated transducer for Model-4 (a) 16·23 mm and (b) 16·13 mm.

Measurement of impedance and resonance frequency of the Model-4 ultrasonic transducer with a geometric configuration of 16·23 mm and a 16·13 mm radiator. The sizes of the main characteristics of this transducer were measured using a Digital Keysight Oscilloscope DSO-X2022A (Figure 14 (a)). This oscilloscope was equipped with a built-in function generator. The measurement transducer was set up using the schematic shown in Figure 14(b). The input sinusoidal voltage given to the piezoelectric ceramic was 1 V_{rms} with a frequency sweep in the range of 18 kHz to 23 kHz, adjusted manually with steps of 10 Hz.

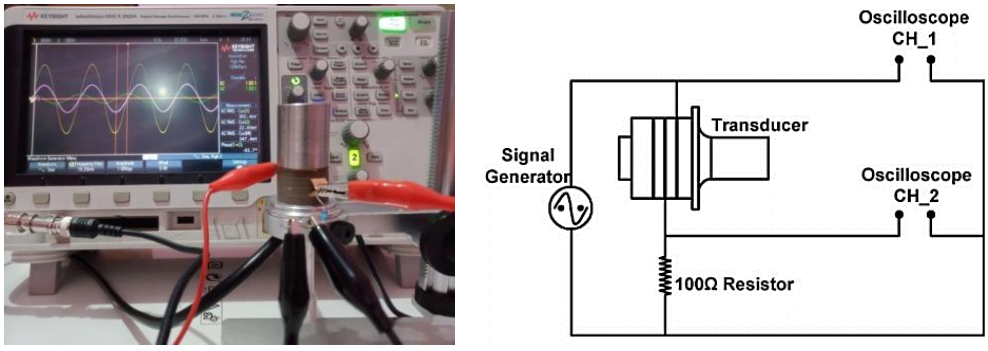

(a) (b)

Figure 14 Setup for measuring transducer characteristics in the experiments: (a) actual measurements using an oscilloscope, and (b) scheme of the measurement set-up [11].

Experiments and Analysis of Model-4

The impedance response measurements of frequency as a function of prestressing forces of 5 kN, 10 kN, and 15 kN for Model-4 with 16·23 mm and 16·13 mm configurations are plotted in Figures 15(a) and (b). Both designs of this Model-4 had relatively the same response. When the applied prestressing force increased, the resonance and antiresonance frequencies increased. Meanwhile, the impedance for the resonance frequency tended to decrease and vice versa for the anti-resonance frequency increases.

In the 16·23 mm Model-4, the resonance frequency increased from 19.43 kHz to 19.56 kHz, while the anti-resonance frequency increased from 19.86 kHz to 19.99 kHz. However, the impedance value at the resonance frequency decreased from 88.37 Ω to 33.23 Ω and increased from 41.19 kΩ to 70.75 kΩ at the anti-resonance frequency. The 16x13 mm model-4 increases the resonance frequency from 19.98 kHz to 20.17 kHz, while the anti-resonance frequency is increased from 20.39 kHz to 20.60 kHz. The impedance value at the resonance frequency decreased from 91.01 Ω to 24.91 Ω, while it increased from 46.84 kΩ to 78.20 kΩ at the anti-resonance frequency.

DOI: 10.5614/j.eng.technol.sci.2023.55.4.1

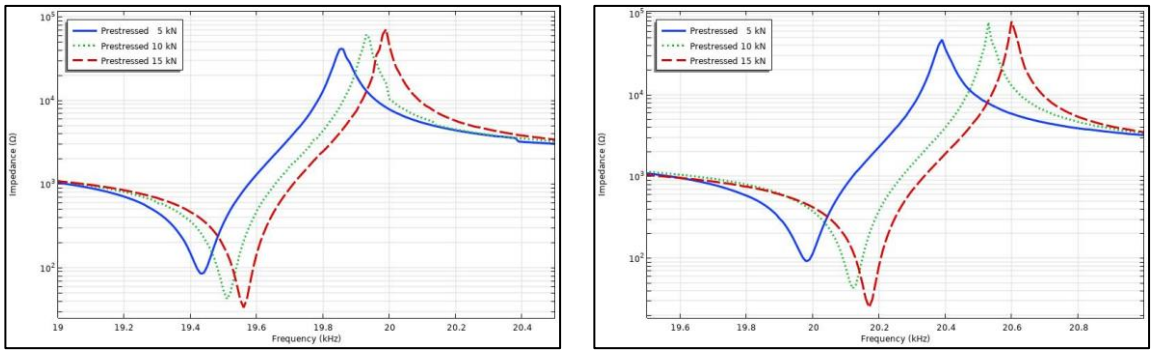

(a) (b)

Figure 15 The results of measuring the impedance vs frequency curve of the transducer for the Model-4 configuration: (a) 16·23 mm and (b) 16·13 mm with 5 kN (blue solid line), 10 kN (green dotted line), and 15 kN (red dashed line) prestressing force.

Table 6 Value of the resonance frequency and impedance and amplitude of the Model-4 vibration at 15kN.

Mode-4 Radiator (mm)	Force Prestressed (kN/Nm)	fr (kHz)	Zr (Ω)	fa (kHz)	Za (kΩ)	Electro-mechanical coupling factor, k_{eff}.
16·23	5/8	1943	84.37	19.86	41.19	0.2070
	10/16	19.51	42.21	19.93	60.95	0.2042
	15/24	19.56	33.23	19.99	70.75	0.2063
16·13	5/8	19.98	91.01	20.39	46.84	0.1995
	10/16	20.12	42.48	20.53	76.03	0.1989
	15/24	20.17	24.91	20.60	78.20	0.2033

Torque force conditions were applied to the bolts for all Model-4 measurements varying from 8 Nm, 16 Nm, and 24 Nm. The average coupling practical value was 0.20. The importance of the transducer characteristics measurement results is shown in Table 6.

Comparison of Simulation and Experiments on Model-4 Transducer

The impedance curve depicting the simulation results with prestress forces of 5kN, 10kN, and 15kN for Model-4, along with configurations of 16·23 mm and 16·13 mm, is presented in Figure 16. The resonant and anti-resonant frequencies, obtained through simulation and experimental analysis for both Model-4 configurations, exhibited a close proximity to the desired resonant frequency of 20 kHz. Notably, for the 16.13 mm configuration of Model-4, the resonant frequency was closely aligned to the target of 20 kHz, as demonstrated by the simulation results of 20.11 kHz, 20.11 kHz, and 20.15 kHz, along with the corresponding experimental results of 19.98 kHz, 20.12 kHz, and 20.17 kHz, respectively, for prestress forces of 5 kN, 10 kN, and 15 kN. Furthermore, the relative percentage errors at the resonant frequency were 0.65%, 0.05%, and 0.10%, while the corresponding values at the anti-resonant frequencies 20.39 kHz, 20,53 kHz, and 20.60 kHz were 1.2%, 0.58%, and 0.34% for prestress forces of 5kN, 10kN, and 15kN, respectively. The effective electromechanical coupling for both the simulation and the experiment was 0.2272, 0.2272, and 0.2229 (simulation) and 0.1995, 0.1989 and 0.2033 (experiment).

Meanwhile, for the 16.23 mm configuration, the resonant frequency was below the target frequency of 20 kHz, as demonstrated by the simulation results of 19.37 kHz, 19.37 kHz, and 19.41 kHz, along with the corresponding experimental results of 19.43 kHz, 19.51 kHz, and 19.56 kHz. Meanwhile, the corresponding values at the anti-resonant frequencies 19.88 kHz, 19.88 kHz, and 18.89 kHz and the experimental results were 19.86 kHz, 19,93kHz, and 19.99 kHz for prestress forces of 5kN, 10kN, and 15kN respectively. The relative percentage error at the resonant and anti-resonant frequency in the simulation were 0.30%, 0.71%, and 0.76%, and 0.1%, 0.25%, and 0.50% for prestress forces of 5kN, 10kN, and 15kN, respectively. The effective electromechanical coupling for both the simulation and the experiment was 0.2251, 0.2251, and 0.2184 (simulation) and 0.2070, 0.2042 and 0.2063 (experiment). Detailed results of the difference between the simulation and the experimental results of the Model-4 transducer configurations 16.23 and 16.13 are shown in Table 7.

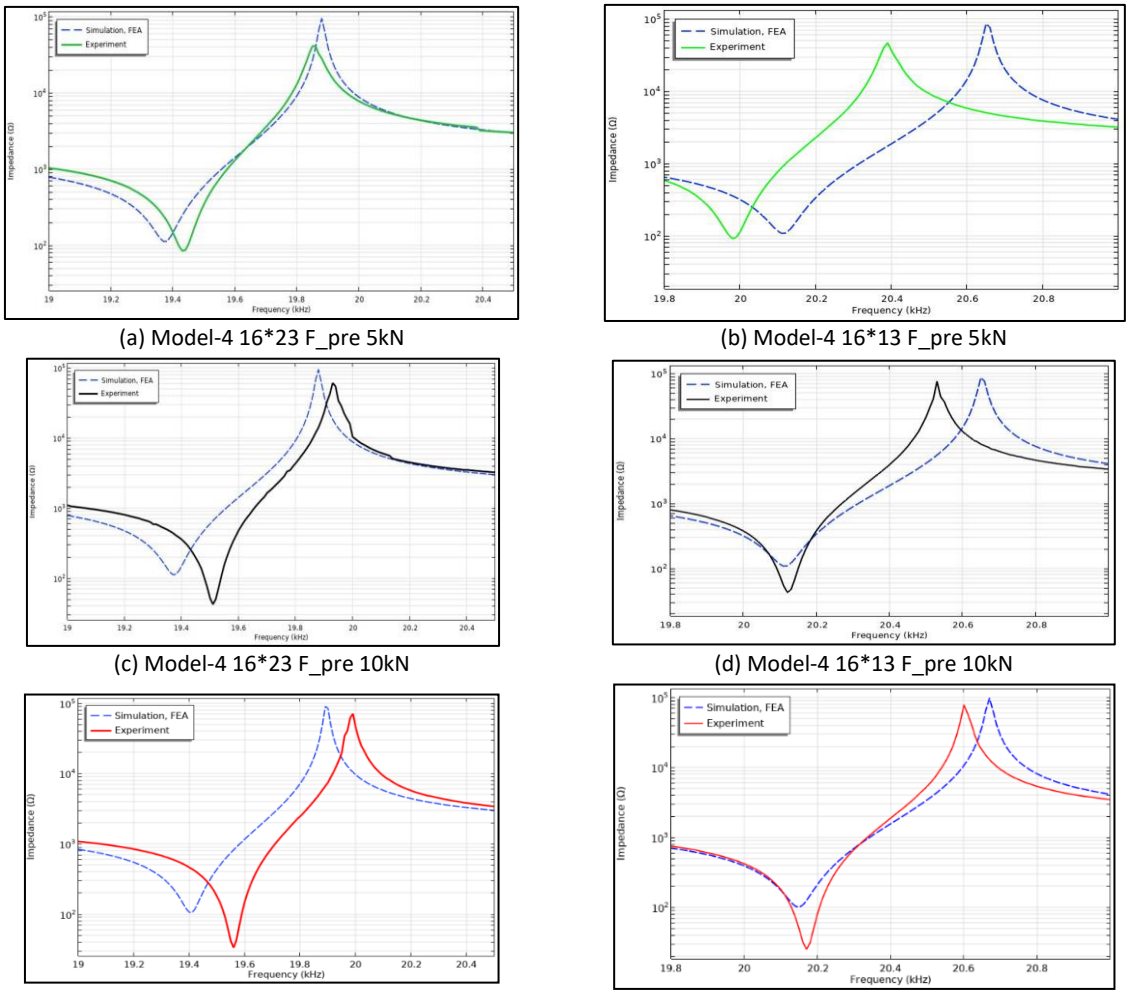

(a) Model-4 16*23 F_pre 5kN (b) Model-4 16*13 F_pre 5kN

(c) Model-4 16*23 F_pre 10kN (d) Model-4 16*13 F_pre 10kN

(e) Model-4 16*23 F_pre 15kN (f) Model-4 16*13 F_pre 15kN

Figure 16 Comparison of simulation to experimental results of impedance vs frequency response for prestressing force at (a) 16·23 mm and (b) 16·13 mm.

Table 7 Value of the resonance frequency and impedance and amplitude of Model-4 vibration.

Model-4 radiator (mm)	Prestress force	f_r (kHz)	Z_r (Ω)	f_a (kHz)	Z_a (kΩ)	Electro-mechanical coupling factor, k_{eff}.
16· 23	Simulation					
	5 kN	19.37	112.11	19.88	95.12	0.2251
	10 kN	19.37	111.93	19.88	94.93	0.2251
	15 kN	19.41	104.97	19.89	89.32	0.2184
	Experiment					
	5 kN	19.43	84.37	19.86	41.19	0.2070
	10 kN	19.51	42.21	19.93	60.95	0.2042
	15 kN	19.56	33.23	19.99	70.75	0.2063
16·13	Simulation					
	5 kN	20.11	107.68	20.65	85.55	0.2272
	10 kN	20.11	107.53	20.65	86.42	0.2272
	15 kN	20.15	100.10	20.67	98.01	0.2229
	Experiment					
	5 kN	19.98	91.01	20.39	46.85	0.1995
	10 kN	20.12	42.49	20.53	76.03	0.1989
	15 kN	20.17	24.91	20.60	78.20	0.2033

DOI: 10.5614/j.eng.technol.sci.2023.55.4.1

Based on the main objective of this study, the transducer structure was dimensioned to achieve a resonant frequency of 20 kHz. The length of each segment or main component, i.e., the front and back mass, was calculated based on a desired resonant frequency of 20 kHz. When comparing the relative errors between the simulation and the experimental results for the Model-4 configurations (16.23 and 16.13), the relative error of 0.76% and 0.1% respectively were obtained at a prestress force of 15 kN. This discrepancy is attributed to the addition of mass to Model-4 with a diameter of 16.23 mm, which resulted in a resonance frequency of 19.41 kHz instead of the expected 20 kHz. However, for Model-4 with a configuration of 16.13 mm, the simulation results closely matched the desired resonant frequency of 20 kHz. Hence, it is crucial to adjust the added mass to the targeted resonant frequency to achieve optimal performance.

Although the relative error was lower (by approximately 0.05%) for the 16.13 mm configuration at a prestress force of 10 kN, it is important to consider the recommended safe pressure range for piezoelectric materials, which is typically between 20 MPa and 40 MPa. The simulation results indicate that when the pretension forces on the bolts were set to 15 kN and the stress distribution on the piezoelectric component to around 40 MPa, based on calculation of the tension on piezoelectric ceramic, fell within the range of approximately 36 MPa, ensuring safe operation and an effective contact area between the transducer's elements.

Conclusions

A series of investigations were carried out to study the design of a BCLT-type transducer model, starting with a Langevin-type transducer with a cylinder constant to a stepped-horn shape on the front mass. The study parameters were changes in the geometric structure, i.e., diameter, fillet radius, and radiator front mass (stepped horn). The total length of the half-lambda transducer was fixed, and the study was varied by applying prestress to the bolts. The resonance frequency and electrical impedance were the main characteristics of the transducer studied. BCLT performance estimation was done using finite element analysis. Prototype Model-4 BCLTs with 16· 23 mm and 16·13 mm configurations were made to validate the simulation results. The percentage difference in the resonance frequency from the simulation and experimental results was 0.76% (Model-4 16· 23 mm) and 0.1% (Model-4 16·13 mm). However, compared to the target resonant frequency of 20 kHz, the percentage differences obtained for each of the four models were 2.2% and 0.85% with prestress at 15 kN. From the results obtained, it can be concluded that a BCLT with a stepped horn front mass with the addition of a radiator segment at the end of the stepped horn can be used to adjust the transducer's resonance frequency appropriately.

Acknowledgments

The author thanks the Lab for Smart Sensors and Actuators, Research Center for Electronics – National Research and Innovation Agency (BRIN) for the support and facilities provided and the manufacturing and measurement processes. The author would also like to thank the GTA program of Institut Teknologi Bandung. This research was partially funded by Institut Teknologi Bandung – PPMI Program 2023.

References

[1] Engelke, D., Oehme, B. & Strackeljan, H.J., *Simulation and Optimization of an Ultrasonic Sandwich Transducer*, International Journal of Advanced Engineering Sciences and Technologies, **8**(2), pp. 203-209, 2011.

[2] Li, X., Stritch, T., Manley, K. & Lucas, M., *Limits and Opportunities for Miniaturizing Ultrasonic Surgical Devices Based On a Langevin Transducer*, *IEEE Transactions on Ultrasonics,* Ferroelectrics, and Frequency Control, **68**(7), pp. 2543-2553, 2021.

[3] Milewski, A., Kluk, P., Kardyś, W. & Kogut, P., *Modelling and Designing of Ultrasonic Welding Systems*, *Archives of Acoustics*, **40**(1), pp. 93-99, Jan. 2015.

[4] Da Silva, J.B., Franceschetti, N.N. & Adamowski, J.C., *Numerical Analysis of a High Power Piezoelectric Transducer Used in The Cutting and Welding of Thermoplastic Textiles*, ABCM Symposium Series in Mechatronics, **2**, pp. 142-149, 2006.

[5] Kim, J. & Lee, J., *Parametric Study of Bolt Clamping Effect on Resonance Characteristics of Langevin Transducers with Lumped Circuit Models*, Sensors (Switzerland), **20**(7), pp. 1-9, Mar. 2020.
[6] Kim, J. & Lee, J., *Theoretical Resonance Analysis of Langevin Transducers with Equivalent Circuit Models for Therapeutic Ultrasound*, Journal of Electrical Engineering and Technology, **14**(6), pp. 2437-2445, Aug. 2019.
[7] Fu, B., Li, T. & Hemsel, T., *A Simple Prestress Estimating Method of Langevin Transducers*, *Symposium on Piezoelectricity, Acoustic Waves, and Device Applications*, SPAWDA, pp. 324-327, 2008.
[8] Arnold, F. J. & Martins, P. S., *New Insights into The Mechanical Prestressing of Piezo Transducers*, Journal of Intelligent Material Systems and Structures**, 32**(8), pp. 867-879, 2021.
[9] DeAngelis, D.A., Schulze, G.W. & Wong, K.S., *Optimizing Piezoelectric Stack Preload Bolts in Ultrasonic Transducers*, Physics Procedia, **63**, pp. 11-20, 2015.
[10] Abdullah, A., Shahini, M. & Pak, A., *An Approach to Design a High Power Piezoelectric Ultrasonic Transducer*, Journal of Electroceramics, **22**(4), pp. 369-382, Jan. 2008.
[11] Baraya, M.Y. & Hossam, M., *Design of an Electromechanical System for Measuring and Monitoring Micro-Ultrasonic Amplitude of Langevin Transducer*, International Journal of Advanced Manufacturing Technology, **107**(7-8), pp. 2953-2965, Feb. 2020.
[12] Haili, J. (ed), *Design and Simulation Analysis of Ultrasonic Extrusion Transducer*, *Proceedings - 2020* 3rd World Conference on Mechanical Engineering and Intelligent Manufacturing, WCMEIM 2020, pp. 802-805, 2020.
[13] Qiao, J. & Wang, F.*, Effect of Tightening Torque on the Frequency of the Sandwich Piezoelectric Ceramic Transducer Vibrator*, Proceedings - 2010 11th International Conference on Electronic Packaging Technology and High Density Packaging*, ICEPT-HDP,* pp. 893–896, 2010.
[14] DeAngelis, D.A. & Schulze, G.W., *Performance of Pzt8 Versus Pzt4 Piezoceramic Materials in Ultrasonic Transducers*, Physics Procedia, **87**, pp. 85-92, 2016.
[15] Pérez-Sánchez, A., Segura, J.A., Rubio-Gonzalez C., Baldenegro-Pérez, L.A. & Soto-Cajiga, J.A., *Numerical Design and Analysis of a Langevin Power Ultrasonic Transducer for Acoustic Cavitation Generation*, Sensors and Actuators A: Physical, **311**(2)**,** 112035, Aug. 2020.
[16] Xu, J. & Huanhuan, R., *Design and Finite Element Simulation of an Ultrasonic Transducer of Two Piezoelectric Discs*, Journal of Measurements in Engineering**, 5**(4), pp. 266-272, Nov. 2017.
[17] He, T., Ye. X. & Zhao, Y., *Optimization Design for Ultrasonic Horn with Large Amplitude Based on Genetic Algorithm*, Journal of Vibroengineering, **17**(3), pp. 1157-1168, Dec. 2014.

Manuscript Received: 20 November 2022
1st Manuscript Revision Received: 29 April 2023
2nd Manuscript Revision Received: 12 June 2023
Accepted Manuscript: 14 August 2023